

Chapter 3

Subcellular Resolution Imaging in Neural Circuits

W. Ryan Williamson, Chih-Chiang Chan, and P. Robin Hiesinger

Abstract

Drosophila combines advanced genetics with a brain of ideal size for high-resolution imaging in toto. However, imaging of intracellular compartments pushes the limits of light microscopy in every system, and at the subcellular level the small size of fly neurons presents a challenge. In this chapter, we review recent imaging advances that, often for the first time, allow the visualization of intracellular biology of neurons in the context of their neuronal circuits. We discuss the different preparations that keep neural circuit architectures intact for live and fixed imaging. Finally, we review advances in light microscopy and imaging probes in combination with these preparations and provide a guide to which high-resolution microscopy techniques are applicable to the different *Drosophila* preparations. We focus on the imaging of intracellular membrane trafficking dynamics. However, since any imaging of intracellular trafficking constitutes an example of imaging at subcellular resolution, many approaches discussed here will be useful for the study of neuronal cell biology in *Drosophila* in general.

Key words: Fluorescent microscopy, High-resolution imaging, Brain dissection, Immunohistochemistry, Live imaging

1. Imaging Approaches in Neural Circuit Preparations

The principle requirements for the visualization of subcellular compartments are the same in all systems: The goal is to visualize distinguishable structures at the highest resolution possible. In addition, live imaging demands minimal phototoxicity. Limits are imposed by both the markers for intracellular proteins and the microscopy technique itself. Recent years have seen the development of many new approaches to high-resolution fluorescence microscopy as well as many new fluorescent probes. The following two sections present recent advances in fluorescence imaging technologies and explain how these technologies can be applied to study subcellular biology in neural circuits in fly preparations in vivo.

1.1. Overview of High-Resolution Fluorescence Microscopy Imaging Approaches

With a steadily increasing number of high-resolution microscope types, the educated choice of which microscope to choose for a specific preparation has become more difficult. For subcellular resolution imaging in living *Drosophila* preparations, we only consider fluorescence microscopy techniques based on far-field high-resolution fluorescence microscopes. Near-field microscopy techniques, like total internal reflection fluorescence (TIRF), are not likely to be useful for imaging neural circuits in vivo due to their lack of working distance (1). There are some applications where conventional light microscopy approaches will be sufficient, but probably none where they would be superior to all high-resolution fluorescence techniques. The basic concept and different incarnations of far-field high-resolution microscopy are described in detail elsewhere (1–3). We only briefly summarize the most applicable approaches for *Drosophila*. In addition, we focus on what microscopy techniques work best with the different preparations.

1.1.1. Conventional Confocal Laser Scanning and Deconvolution

The traditional point-scanning confocal microscope has been the most widely used high-resolution fluorescence microscopy technique for over 15 years. With excellent optics, the resolution of today's laser scanning microscopes indeed closely approaches the diffraction barrier with 250 nm in the x/y plane and 600 nm in the z axis (light path through the lens). The theoretical resolution limit in the x/y plane is given by half the excitation wavelength, i.e., 244 nm for a 488 Argon laser line (GFP illumination), and 316.5 nm for a 633-nm Helium–Neon laser line (far-red, e.g., Cy5, illumination). The resolution limit in the z axis is more than twice that of x/y and described by the *point spread function (PSF)*. The PSF is a mathematically defined description of the detectable light spread from a point light source (4). In three-dimensional (3D) space, this spread has the shape of a rocket along the z -axis (Fig. 1). If the point from which the spread originates and the shape of the PSF are known, then the PSF can be transformed back into a point for the purpose of removing light scatter and out-of-focus light in confocal datasets. This is the principle of *deconvolution* (5, 6). *Nonblind deconvolution* utilizes a measured PSF (as shown in Fig. 1a), whereas blind deconvolution assumes a simple PSF (e.g., Gaussian) and then tests every voxel in a 3D dataset for whether this PSF is indeed applicable—altering the image data and PSF in turn in an iterative computation-intensive process (e.g., (7)). As shown in Fig. 1, the “point spread” inside a *Drosophila* brain is inhomogeneous and therefore limits the applicability of the same PSF for every point in a 3D or 4D dataset (7). Deconvolution brings the data closer to the resolution limit by removing artificial light scattering introduced by the optics and the preparation itself. However, deconvolution does not remove the diffraction barrier. The principle of deconvolution will become more important in the

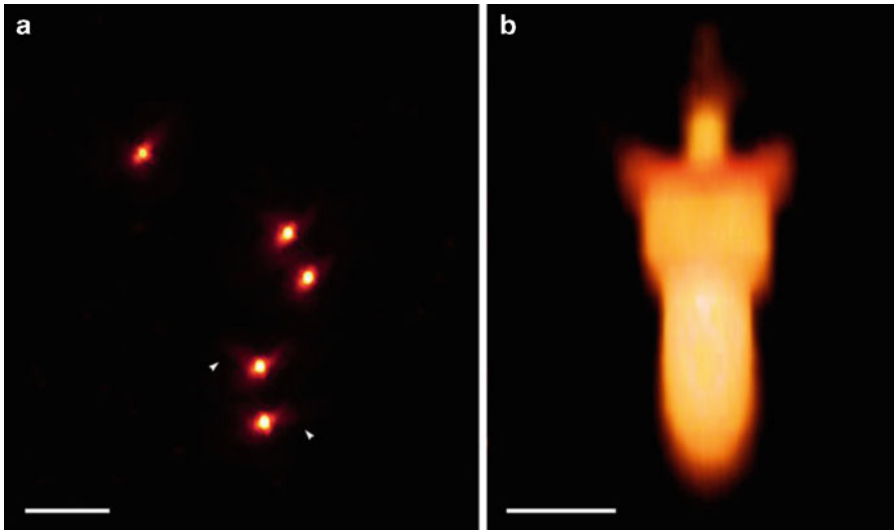


Fig. 1. A point in the confocal microscope. **(a)** 500-nm fluorescent beads that were injected into a fluorescently immunolabeled adult *Drosophila* brain and scanned with a conventional confocal microscope at 20 μm depth (7). All five beads show different light scattering due to unpredictable tissue-dependent distortions of the point spread function (PSF). **(b)** Volume rendering of a three-dimensional (3D) conventional confocal scan of one of the beads shown in **(a)**. The light path to the lens is up. Such scans of a perfectly round object show the principle shape of the PSF for fluorescent point minus further tissue-dependent distortions as shown in **(a)**. Scale bars in **(a)** 5 μm , in **(b)** 1 μm .

section on superresolution imaging techniques that effectively remove the diffraction barrier for visible light (1). For conventional confocal microscopy datasets numerous powerful software implementations exist that can be used independently of the microscope with which the data was obtained.

Confocal microscopes have the very useful ability to optimize the imaging and resolution setting for each lens and specimen size by adjusting several parameters. In practice, one wants to use the lens with the highest numerical aperture possible, adjust the confocal pinhole to an airy disc of 1 or just slightly above 1, and finally digitally zoom to adjust the scan area to match the pixel size to the resolution limit. The principle of the confocal pinhole is discussed elsewhere (2); here, it shall suffice to note that an airy disc of 1 defines the point of maximum confocality; below this value light is further lost without gaining resolution in the z axis. In contrast, an airy disc above 1 increases light detection by opening the pinhole and losing “confocality,” i.e., resolution in the z axis. In the x/y plane, it is rarely useful to increase digital zoom such that the pixel size falls below 100 nm (e.g., 50 μm^2 for a 512 \times 512 pixel scan). Note that any scan resolution below the diffraction limits of 200–250 nm (i.e., any scan of less than 100 μm^2 at 512 \times 512) is theoretically empty resolution and only helpful as a means of “spatial averaging,” which is an application-dependent alternative to temporal averaging, i.e., rescanning the same points several times (see below).

For live imaging purposes, the second major set of parameters to consider are the scan speed and dwell times. Conventional confocal microscopes operate by point-scanning and digitally integrating pictures from scanned lines. This is a slow process and the speed depends on how fast the point-scanner moves. The standard galvanometer scanning mirror in confocal microscopes operates between 400 and 1,000 Hz. Hence, a single-channel 512×512 image (without averaging) will take between 0.5 and 1 s. If timing permits, averaging should always be used as it dramatically improves image quality by averaging out random noise. Using $\times 4$ line or frame averaging of a 512×512 pixel scan in a single channel will therefore take around 2 s to obtain. A 3D dataset of $512 \times 512 \times 64$ voxels will therefore take 128 s per channel. Importantly, the slow video rate is not the only problem of slow scan speed. Slower point-scanning also means longer dwell times of the laser on fluorophores which greatly increases photobleaching and phototoxicity (3, 8).

1.1.2. Resonant Scanning and Spinning Disc Confocal

Both Resonant Scanning and Spinning Disc Confocal Microscopes overcome the slow scan speed of conventional confocal microscopes. The resonant scanning technique is based on the ability of a galvanometer mirror to operate at a resonant frequency that is approximately ten times higher than its normal scan speed (e.g., 8,000 Hz). Technically, this is achieved by sending a sine wave control function to the galvanometer motor. The $\times 10$ acceleration is sufficient to turn a point-scanning confocal into a real live imaging microscope with substantially reduced phototoxicity and scan speed at video rates. A 512×512 pixel scan takes 0.05–0.1 s, i.e., up to 20 frames per second (fps) at 512×512 , 512×256 or 256×256 scans are twice as fast. Averaging can be applied to increase image quality at the expense of speed. Dramatic increases of averaging (e.g., $\times 32$ or $\times 64$) yield the same quality high-resolution images as conventional confocal microscopy at the same slow speed—but with one major difference: photobleaching and phototoxicity are substantially reduced due to much shorter dwell times of the point scanner at the time of excitation (8). The disadvantage of the resonant scanner over the conventional microscope is that the ability to adjust the scan speed and regions of interest are lost. In almost all other aspects, a resonant confocal is identical to the conventional confocal. Bimodal microscopes have been available for several years.

The spinning disc confocal microscope is based on an architecture different from that of conventional point scanners. The principle is reviewed in many excellent references (9, 10). We focus on the differences with respect to typical *Drosophila* imaging preparations. In brief, Spinning Disc microscopes use a quickly rotating so-called Nipkow-Disc with defined pinhole size (the pinhole can only be changed by exchanging the Nipkow Disc). Illumination does not require a laser and photon detection is done with a fast

charge-coupled device (CCD) camera. Despite these major differences, spinning disc microscopes are true confocal microscopes in that out-of-focus light is largely blocked from reaching the detector through, in this case, many confocal pinholes. However, the image is not “scanned” and does not need to be digitally integrated as would be required with laser scanning confocal microscopes; the CCD camera indeed “sees” the whole visible field at a fast video rate. The major limitation of this technique is that some out-of-focus light still reaches the detector through adjacent pinholes (so-called pinhole cross talk). The problem increases with the depth of the tissue under investigation and causes depth-dependent loss of confocality. In addition, illumination that does not pass through the pinholes can get reflected by the disc resulting in higher background noise. Finally, spinning discs do not offer any of the advantages that come with laser point-scanners, like photo-bleaching or photoactivation in small regions of interest.

1.1.3. Multiphoton Microscopy

A key parameter that we have so far not discussed is the working distance: How deep can I scan? Multiphoton microscopy addresses this issue by using far-red excitation lasers that penetrate deeper into tissue with less light-scatter. The basic concept is that photon density reaches a threshold for excitation only in the focal plane, thereby completely eliminating out-of-focus excitation. Since only one point is illuminated, no confocal pinhole is required to eliminate out-of-focus light. The focused excitation also dramatically reduces phototoxicity due to unproductive excitation. Multiphoton microscopy techniques are reviewed elsewhere (2, 11). It should be noted that multiphoton microscopes are diffraction-limited similar to other light microscopes; indeed, they have a theoretically reduced maximal resolution due to the long excitation wavelength. In practice, however, the ability to exclude out-of-focus excitation, especially in deep tissue, often yields higher resolution data than confocal microscopes in similar circumstances. Examples of multiphoton microscopy are discussed in the following sections.

1.1.4. Far-Field Superresolution-Imaging with STED and PALM/ STORM

The diffraction barrier described by the formula of Ernst Abbe in 1873 dictates that two simultaneously illuminated points (or fluorescent molecules) must be separated by at least a distance of half the wavelength of light in order to be resolved. The shorter wavelength of an electron similarly defines the resolution limit of electron microscopy. Only within the last few years have widely applicable fluorescent microscopy techniques become available that effectively break the diffraction barrier (3, 12). All techniques are based on the idea that two fluorescent molecules that are closer together than 200 nm can be excited sequentially. In other words, they are not separated spatially, because diffraction cannot be removed per se, but temporally. However, the technical hurdles of exciting two fluorophores separately within 200 nm are

substantial, simply because no lens-focused beam of light illuminates a spot smaller than 200 nm. Different techniques have emerged in recent years that achieve superresolution imaging with different approaches. Two approaches have become available for practical usage in the last few years: stimulated emission depletion (STED) microscopy and photoactivatable localization microscopy (PALM) or stochastic optical reconstruction microscopy (STORM). The technical details of these techniques are discussed elsewhere (1, 3). Here, we focus on the basic principles and differences that serve as a foundation for the choice of application in *Drosophila*.

STED is based on confocal point-scanning microscopy; indeed, the first commercially available STED setup can be obtained as an upgrade to an existing confocal laser scanning microscope. The basic trick is a red-shifted so-called STED laser that illuminates in a donut shape around the standard excitation point laser. Wherever the STED laser provides sufficient energy fluorescence is suppressed due to the photophysical property of stimulated emission. The “hole” in the middle of the STED laser is characterized by a gradient of decreasing STED laser energy. With increasing STED laser intensity the hole becomes smaller and only fluorophores that are below a photophysical threshold become excited by the excitation laser. By point-scanning with the excitation/STED laser pair in an otherwise conventional confocal setup, neighboring fluorophores that are closer together than 200 nm can be sequentially activated and thus resolved.

PALM/STORM microscopy uses a radically different approach to temporally separate two fluorophores within 200 nm: sparse illumination (13, 14). In effect, both PALM and STORM use threshold illumination that randomly illuminates fluorophores in a specimen such that typically no fluorophores within a 200 nm radius are illuminated at the same time. If a sparsely illuminated fluorophore emits enough photons, its location can be determined using the same principle described above for deconvolution. The key difference between STED and PALM/STORM therefore is this: With STED the microscope “knows” where every single photon comes from, whereas in PALM/STORM its location needs to be determined. Few photons from a fluorescent molecule suffice to determine its localization in STED, but it must be capable of repeating many on/off cycles through stimulated emission. In contrast, in PALM/STORM any given fluorophore may theoretically only have to be excited once, as long as it emits enough photons to deconvolve its localization. In practical terms, this has led to a greater applicability of PALM/STORM for more fluorescent molecules. STED, on the other hand, is currently the faster method for live imaging. The development of these approaches is very fast-paced, and increasing speed and applicability can be expected for both types of systems at the time of publication.

1.2. What Microscopy Technique Should I Use for My Preparation?

1.2.1. Considerations for Choosing the Right Microscopy Technique

Consideration 1: Live or Fixed?

In the following section, we review the applicability of the above described microscopy techniques for *Drosophila* preparations that are useful for imaging of neural circuitry. The following considerations apply:

Conventional confocal laser-scanning microscopy still offers the greatest versatility for imaging fixed preparations for the size of the *Drosophila* brain. However, at high resolution and with weak fluorescence (and consequently high laser intensities) photobleaching becomes a serious issue. In such cases, resonant-scanning helps by decreasing photobleaching at the cost of losing some versatility (mainly a smaller minimal field of view and no scanning of asymmetric regions of interest).

Spinning Disc, Resonant Scanning, and Multiphoton confocals are all suitable for live imaging due to their reduced phototoxicity. However, they achieve this by three different means—weak nonlaser illumination for the spinning disc, reduced point-laser dwell time for the resonant confocal, and reduced out-of-focus excitation in the case of multiphoton. We are not aware of a direct comparison of the three for the same preparation and we do not have high-end spinning disc or multiphoton microscopes available to perform this comparison. However, information from successful experiments in *Drosophila* preparations together with knowledge of the different architectures of these microscopes allow several conclusions to be drawn regarding what should and should not work. As outlined above, if the tissue depth is small and imaging close to the diffraction barrier is not required, spinning disc confocal microscopy is still a good choice. Recent work on imaging the development of the *Drosophila* wing imaginal disc offers some details that should be applicable to neural circuit preparations (15). In addition, a video protocol is available for another preparation that only requires a small working distance using spinning disc microscopy (16).

Resonant scanning has become more popular in recent years as an extension of the applicability of conventional confocal laser scanning microscopes. We have recently used resonant scanning for live imaging in developing eye disc–brain culture (17, 18). For high-resolution far-field imaging, we use a $\times 63$ (NA 1.3) glycerine lens that increases the working distance by more than 10 μm compared to oil immersion lenses. However, light scattering deeper than 20 μm in the *Drosophila* tissue in water precludes high-resolution imaging. Furthermore, even strong fluorophores require averaging between $\times 8$ and $\times 48$ to reduce noise. More details are available in a video protocol (18).

Multiphoton microscopy has been very successfully applied in a number of *Drosophila* brain preparations, including live imaging of the olfactory lobe (19, 20), and is discussed below in the context of the adult brain preparation.

Consideration 2: How Deep
Do You Need to Image?

The fluorescent microscopy techniques discussed above allow for quantitative imaging in deep tissue in the following order: Multiphoton > Resonant Confocal & STED > PALM/STORM > Spinning Disc. Successful application of spinning disc confocals is largely restricted to cell culture and thin preparations where tissue within only a few micrometers of the surface is imaged (e.g., (16)). In the case of *Drosophila* preparation, subcellular high-resolution imaging of structure deeper than 10 μm is most likely better performed using a resonant scanner. We routinely use resonant scanning for live pupal and adult brain preparations up to depths of 20–30 μm (18). Below a tissue depth of 20–30 μm multiphoton approaches provide significantly higher quality data.

Consideration 3: How
Weak Are Your Fluorescent
Probes?

Both the CCDs in spinning disc confocals and the photomultiplier tubes (PMTs) in line-scanning confocals are single photon detection devices. The biggest differences are speed and light-sensitivity: The PMT is the fastest available photon detector, generating an electrical output after photon detection within a few nanoseconds (providing the key reason for its use in line-scanning microscopes). With respect to light-sensitivity (and almost all other parameters), today's newest CCDs outperform PMTs. The quantum efficiency (i.e., probability of a single photon to cause a detectable charge) is 5–20% for PMT and 25–95% for CCDs. In addition, CCDs have a dynamic range ten times as large as those of PMTs as well as less dark signal and noise.

Consideration 4: How Fast
Do You Need to Image?

CCD-based imaging is faster, simply because the CCD sees the whole image at any time point whereas line-scanning is very time costly. Hence, most imaging purposes that require an imaging rate of more than 25 frames per second are CCD-based (including the spinning disc confocal). For image rates below 25 frames per second many other considerations start to play a role for the choice of microscope. While a resonant confocal offers most of the advantages and flexibility of a full confocal microscope, the image quality increases only with lower speed. Where the speed/quality curves intersect depends on many parameters, including the brightness of the fluorophores. In practical terms, a high-resolution resonant scan at 25 frames per second will in most cases be too noisy for subcellular imaging. We typically need to average at least $\times 8$ to discern subcellular structures in *Drosophila* brain or filet preparations below 500 nm in x/y , making the fastest reasonable speed for a single 512×512 scan 3 frames per second.

Consideration 5: How Long
Do You Need to Image?

Long live imaging sessions (hours and longer) suffer from two main problems: drift and phototoxicity/photobleaching. Phototoxicity is discussed in Consideration 1. Drift originates from both movements of the preparation as well as the microscope. High-quality stages guarantee focus drift of less than 1 μm in the

z direction per hour. Key to reducing microscope/stage drift on any system is to keep the temperature constant. Ideally, the microscope should be running for 2 h at least to reach an even operating temperature of all parts, especially for *Drosophila* preparations which do not require a heated stage or chamber. Drift is negligible in x/y for high-performance microscope stages and less in z for 2D imaging over time. For 3D imaging over time, a galvanotable with nanometer accuracy inside the stage is highly recommended. Drift of the preparation within the imaging chamber can be very difficult to control and are inherent for a moving (e.g., some filet preparations) or developing specimen (e.g., the eye–brain complex). Where some drift is unavoidable the simplest solution is to choose a generous bounding box, i.e., imaging a region with sufficient space around the region of interest to allow for a certain amount of drift. Several software solutions exist for realignment of 3D datasets. In addition, several smart integrated software/hardware solutions have recently been developed that can track and correct for preparation drift by automatically correcting stage positioning during long live imaging sessions. All of these options can be explored thoroughly with the major microscope and imaging software manufacturers.

With these considerations in mind, the following *Drosophila* “neural circuit” preparations are available for imaging:

1.2.2. Embryo

The embryonic central nervous system develops within a few hours and becomes functional only an hour before the embryo hatches. The embryonic CNS has therefore mostly been studied as a model for early nervous system development. The early brain and ventral ganglion are too deep inside the intact embryo (20–60 μm) for live imaging with spinning disc microscopy. Resonant scanning allows deeper imaging, but no high-resolution scanning deeper than 20 μm is possible. Beyond this depth, multiphoton is recommended. For fixed tissue, conventional confocal works very well in cleared tissue, as it allows high-resolution scanning through approximately half the thickness of the intact embryo (50–75 μm).

An alternative to the intact embryo is the embryo filet in which the CNS as well as all neuromuscular junctions (NMJs) are directly exposed (Fig. 2a). The preparation of embryo filets is made possible by water-polymerizing surgical glues (21). Imaging can be performed either using a water-dipping lens or inside a perfusion chamber (18). A high-resolution water-dipping lens can greatly improve the quality of live imaging of both the CNS or the NMJs using spinning disc or resonant confocal microscopes.

1.2.3. Larval Eye Disc–Brain Complexes

The larval brain-imaginal discs complex is easily dissected from third instar wandering larvae (18). The developing imaginal disc sends hundreds of photoreceptor axons into the larval brain hemispheres through the optic stalk; the leg discs are innervated by axons from the larval brain. Hence, the larval brain-imaginal disc

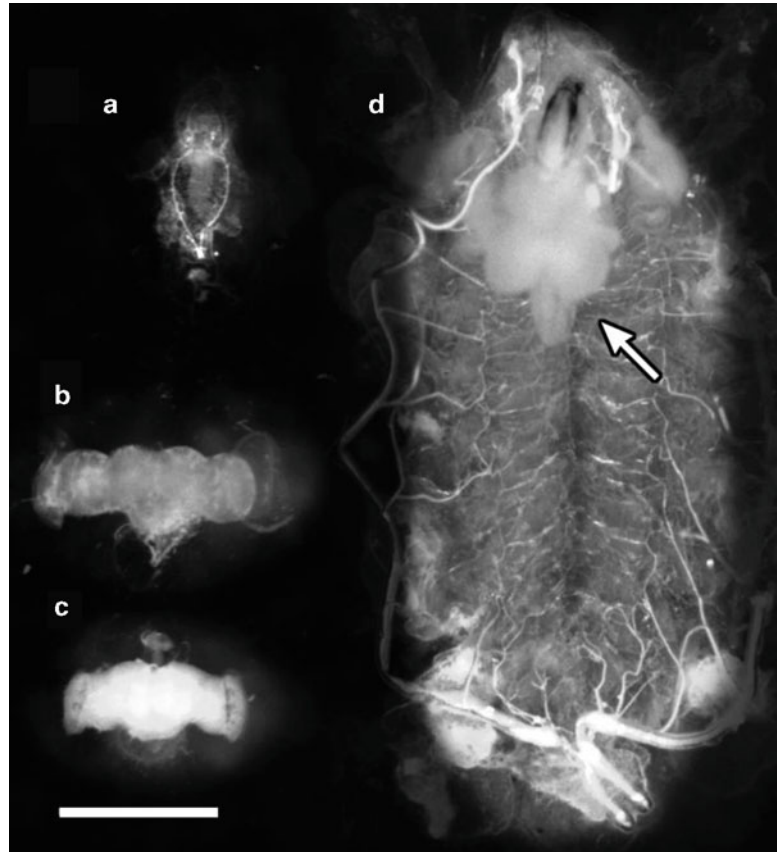


Fig. 2. *Drosophila* live neural circuit preparations. (a) Embryo file preparation. (b) Pupal P+30% eye-brain preparation. (c) Adult brain. (d) L3 larval file preparation. The larval brain-eye disc complex is marked with an *arrow*. Scale bar: 500 μm .

complex is an excellent model for neural circuit formation *in vivo*. Live imaging can be performed in a perfusion chamber using resonant confocal microscopy (18). The size and thickness of the larval brain are comparable to those of a whole-mount embryo (comp. Fig. 2a and arrow in 2D). Hence, all considerations discussed above for the intact embryo preparation apply.

1.2.4. Larval Filet

The larval filet preparation (Fig. 2d) has served as the work horse of synapse function and plasticity studies in *Drosophila* for more than 20 years. The larval filet presents an *in vivo* setting that is amenable to electrophysiological and imaging studies of the NMJ. The NMJs are large (up to 5 μm) bouton-like synaptic contacts between the motor neurons that originate in the ventral ganglion and the body wall musculature of the larva. The larval filet can be handled very similar to neuronal cell culture systems in terms of accessibility to bath solutions, dyes, and electrodes. Since the complete nervous system remains intact, the larval filet represents

an ideal preparation for the study of motor neuron circuitry *in vivo*. Like the embryo filet, the larval filet can be prepared either using water-polymerizing surgical glue and imaged in a closed perfusion chamber, or (more commonly) with a water-dipping lens. In the latter case, the preparation is typically performed using small metal pins to immobilize the living preparation. The larval filet is amenable to high-resolution imaging with any live imaging technique (including spinning disc and resonant scanning) due to the direct exposure of the nerves and synaptic boutons in the preparation. Finally, superresolution imaging has been applied very successfully with this preparation (22).

1.2.5. Pupal Brain

The pupal brain (including the developing eyes) is an excellent preparation for the study of neural circuit development (Fig. 2b). During 20–40% of pupal development, the eye–brain complex is largely detached from other structures in the pupa as it undergoes metamorphosis. The dissection is easy and live imaging can be performed in a closed perfusion chamber (18). The first successful brain culture of the developing pupal brain was performed by Gibbs and Truman (23). Live imaging of development is difficult and few examples are available. Recent developments for the imaging of the wing disc may be helpful (15) as are optimized techniques for culture media and perfusion (18, 24).

1.2.6. Adult Brain

The adult *Drosophila* brain (Fig. 2c) is currently at the forefront of the quest to unravel neural circuitry *in vivo*. The adult fly brain is only a little bigger than the whole-mount embryo; hence, most imaging techniques for the embryo are applicable to the adult brain. There are a plethora of genetic driver and expression probes available to image the circuit function at the cellular and subcellular level. The main focus of the last few years has been on the olfactory and visual systems as well as central brain structures implicated in learning and memory, especially the mushroom bodies. With the possible exception of the first optic neuropil, the lamina and the glomeruli of the olfactory lobes, most adult brain structures of interest require some working distance and capability to perform high-resolution scanning at depths greater than 20 μm . Indeed, successful live imaging of neuronal activity in the olfactory lobe has been made possible by multiphoton microscopy (19, 20, 25). Although resonant scanning should theoretically perform similarly in this system, we are not aware of a comparable study. In addition, it is likely that STED and PALM/STORM will prove very useful in the study of neural circuitry in the adult brain, as both allow superresolution imaging with an increased working distance compared to conventional confocal microscopy (3). The visual system has proven especially useful with respect to subcellular resolution imaging of neurons *in vivo*. This is mostly because photoreceptor neurons have large and easily accessible cell bodies in the developing

eye epithelium and require little working distance. Similarly, photoreceptor synaptic terminals are comparably large (cylindric shape of 1 μm diameter and more than 10 μm length). These synaptic terminals require imaging between 10 and 30 μm deep inside tissue in an intact brain preparation. However, a special eye preparation with the first optic neuropil (but not the remaining optic lobe) attached allows imaging of live photoreceptor terminals with less than 5 μm tissue depth (17, 18). In addition, numerous genetic tools are available for the photoreceptor-specific expression of fluorescent subcellular probes. Finally, both the photoreceptors and their postsynaptic targets can easily be genetically manipulated (26–28). Similar tools are available for the manipulation of the olfactory lobes and other brain structures.

2. Working with Fluorescent Reporters in Neural Circuit Preparations

Fluorescent reporters can be used to assay the size and location of subcellular compartments, the spatial and temporal dynamics of a compartment and the characteristics of the subcellular environment such as pH. This section includes reporters that have either proven useful in *Drosophila* preparations or suggest themselves for experiments in neural circuit preparations based on experiments in other systems (Table 1). We do not provide detailed protocols for the precise methods for implementing each technology. Instead, we focus on the key features and practical information for the application of the different fluorescent reporters in imaging neural circuit preparations.

2.1. Targeted Labeling

The following fluorophores have a single absorption/emission spectrum (i.e., nonphotoconvertible, nonphotoactivatable) and are used to tag proteins of interest with the primary purpose of determining protein localization. We focus on relatively new or otherwise special probes and do not discuss commonly used xFP-type fluorescent proteins.

2.1.1. mKate2

Most standard confocal microscope setups include a far-red laser (e.g., HeNe 633 nm) for the visualization of far-red fluorescent probes. Commonly used fluorescent probes in the far-red spectrum include Cy5TM-conjugated antibodies and the nuclear dye TOTO-3TM. Together with blue laser excitation (GFP range) and green laser excitation (RFP range) the far-red spectrum is the most common choice for simultaneous imaging of a third channel. Nonetheless, the development of genetically encoded far-red fluorescent tags has been slow. For several years mPlum served as far-red fluorophore, although its excitation maximum of 590 nm (emission max. at 649 nm) is red-shifted by a large amount and its quantum yield and photostability are inferior to those of most xFPs.

Table 1
Selected Fluorescent Reporters for the Analysis of Neural Circuit Preparations

Sections Class	Fluorophore	Activation wavelength	Reversible	Before activation		After activation		Primary mode of introduction	Useful imaging technologies	References
				Emission max (nm)	Excitation max (nm)	Emission max (nm)	Excitation max (nm)			
2.1	mKate2	n/a	n/a	n/a	588	633	Gene	Conv, STED	(29)	
	EBFP2	n/a	n/a	n/a	383	448	Gene	Conv	(30)	
	FLAsH	n/a	n/a	n/a	510	535	M-P tag	Conv	Invitrogen.com	
	ReAsH	n/a	n/a	n/a	593	607	M-P tag	Conv		
	KillerRed	n/a	n/a	n/a	585	610	Gene	Conv	(36)	
2.2	Photoconvertable	405	No	458	458	520	Gene	Conv	(38)	
	Dendra2	405, 488	No	490	553	573	Gene	Conv	(39)	
	Photoactivatable	405	No	n/a	564	595	Gene	PALM/STORM	(41)	
	Dronpa	405	Yes	n/a	503	518	Gene	PALM/STORM	(42)	
	bsDronpa	405	Yes	n/a	460	504	Gene	PALM/STORM	(45)	
	Cyanine dyes	350–570	Yes	n/a	647	665	IHC	PALM/STORM	(46)	
		350–570	Yes	n/a	746	773	IHC	PALM/STORM		
	Rhodamine amides	375	Yes	n/a	Green	545	IHC	PALM/STORM	(47)	
		375	Yes	n/a	Green	552	IHC	PALM/STORM		
		375	Yes	n/a	Green	577	IHC	PALM/STORM		
	375	Yes	n/a	Green	617	IHC	PALM/STORM			
2.3	Quantum dots	n/a	n/a	n/a	Various	Various	Endo	Conv, 2-Photon, STED	Invitrogen.com	
	pHrodo	n/a	n/a	n/a	560	585	M-P dye	Conv	Invitrogen.com	
	FM 1-43	n/a	n/a	n/a	510	626	M-P dye	Conv, 2-Photon	Invitrogen.com	
	FM 4-64	n/a	n/a	n/a	558	734	M-P dye	Conv		

(continued)

**Table 1
(continued)**

Sections Class	Fluorophore	Activation wavelength	Reversible	Before activation		After activation		Primary mode of introduction	Useful imaging technologies	References
				Excitation max (nm)	Emission max (nm)	Excitation max (nm)	Emission max (nm)			
2.4	LysoTracker	n/a	n/a	n/a	373	422	M-P dye	Conv	Invitrogen.com	
		n/a	n/a	n/a	504	511	M-P dye	Conv, 2-Photon		
Lysosensor	Red DND-99	n/a	n/a	n/a	577	590	M-P dye	Conv		
	Blue DND-167	n/a	n/a	n/a	373	425	M-P dye	Conv	Invitrogen.com	
	Green DND-189	n/a	n/a	n/a	443	505	M-P dye	Conv, 2-Photon		
	pHluorin	n/a	n/a	n/a	475	508	Gene	Conv	(66)	
	HyPer	n/a	n/a	n/a	500	516	Gene	Conv, 2-Photon	(67)	
	GCaMP3	n/a	n/a	n/a	490	520	Gene	Conv, 2-Photon	(85)	
	CuFL	n/a	n/a	n/a	503	525	Gene	Conv, 2-Photon	(73)	

Gene genetically encoded; *M-P tag* membrane-permeable tag; *IHC* immunohistochemistry; *Endo* endocytosis; *M-P dye* membrane permeable dye

mKate2 is a monomeric, bright, and very photostable genetically encoded far-red fluorophore that represents an improved version of the previously developed TagFP635. It is reportedly threefold brighter than TagFP635 and tenfold brighter than mPlum (29). Expression of this protein has been demonstrated in *Xenopus* embryos and in mammalian cell lines but not to our knowledge in *Drosophila*. We have previously generated transgenic flies expressing proteins tagged with TagFP635. In our hands, this probe is sufficiently bright in the far-red spectrum, but exhibited significant overlap with probes in the green laser/red emission channel. The reported excitation maximum for mKate2 is 588 nm, with an emission maximum at 633 nm. Like mPlum, this probe is therefore best excited with an orange laser, but not a far-red (633 nm) laser. At this point, the development of a true far-red fluorescent tag is still outstanding.

2.1.2. EBFP2

Fluorophores that can be excited with ultraviolet lasers and fluoresce in the blue spectrum allow to add channels using shorter (blue-shifted) wavelengths in conjunction with fluorophores in the main visible spectrum (GFP-RFP range). The blue fluorescent protein EBFP2 has an excitation peak at 383 nm and maximum emission at 448 nm. It is therefore ideal for simultaneous imaging with GFP and higher wavelength fluorophores (30). However, EBFP2 forms weak dimers and is therefore of only limited use as a protein tag. Expression of myr-EBFP2 has been demonstrated in *Drosophila* neurons (31).

2.1.3. FAsH and ReAsH

Bulky genetically encoded fluorophores can interfere with the function or localization of proteins. A possible solution is the use of small-molecule dyes that associate with high affinity with a short, nonbulky genetically encoded tetracysteine motif Cys–Cys–Pro–Gly–Cys–Cys. FAsH and ReAsH are biarsenical compounds that must be added exogenously to the preparation (32). These small molecules are easily dissolved in culture media and diffuse freely across membranes. This allows the imaging of protein localization in vivo using small tags and a small fluorescent molecule. However, this technique relies on diffusion of the fluorescent molecule into cells that are directly exposed to the culture medium. FAsH maximally excites at 508 nm and maximally emits at 528 nm. ReAsH maximally excites at 593 nm and emits at 608 nm.

An additional key use for FAsH labeling is acute inactivation of the protein associated with the FAsH molecule, a technology termed FAsH-FALI (fluorophore-assisted light inactivation). At the *Drosophila* NMJ, the technique has been used with success to assay an endocytic function of Synaptotagmin during the synaptic vesicle cycle (33, 34). This technology was recently applied using recombinering-mediated insertion of the tetracysteine motif into a gene locus within a large genomic fragment, thereby eliminating the

problems associated with over-expression of a construct via the Gal4/UAS system (33, 35). For more information about FIAH-FALI, see Chap. 6.

2.1.4. KillerRed

KillerRed is a genetically encoded red fluorescent fluorophore that has been selected for maximal production of reactive oxygen species (ROS) (36). Light-induced reactive oxygen production leads to a dosage-dependent inactivation of neighboring proteins and subsequently the cell death. KillerRed forms dimers, limiting its use as a protein tag. Successful KillerRed-induced cell ablation has recently been reported in neural circuits of zebrafish (37). We have generated *Drosophila* strains for the expression of KillerRed, including expression of cytosolic KillerRed (UAS-KillerRed) as well as tagged neuronal intracellular trafficking proteins neuronal Synaptobrevin and V100 (unpublished data and (17)). All probes serve as excellent red fluorescent probes in *Drosophila* preparation. However, we have so far not succeeded in effecting any phototoxic effect with either green light or laser activation in *Drosophila*.

2.2. Photoactivation/ Photoconversion

Photoactivatable fluorescent proteins (PAFPs) are nonfluorescent until stimulated by an activating wavelength of defined intensity. After activation, PAFPs exhibit specific excitation/emission spectra. Photoconvertible FPs (PCFPs) exhibit a particular excitation/emission spectrum until excited by a specific wavelength of light that results in a shift of the emission maximum. The following PAFPs and PCFPs are applicable for live imaging and superresolution fluorescent microscopy.

2.2.1. Phamret

Phamret is an acronym for Photoactivation-mediated resonance energy transfer. This probe couples PA-GFP to a high-performance ECFP variant through a two amino acid linker. It is a PCFP that can be excited at the pre- and postphotoconverted state with the same excitation maximum at 458 nm, resulting in cyan fluorescence before photoconversion and PA-GFP emission after conversion. Photoactivation is effected with 405-nm illumination to evoke FRET between the ECFP moiety and activated PA-GFP. After photoactivation, Phamret exhibits green fluorescence with an emission maximum at 520 nm. One of the advantages of Phamret is the use of a single excitation wavelength before and after photoactivation. Since only one laser is required for imaging, this PCFP can be used to determine protein diffusion kinetics up to $100 \mu\text{m}^2/\text{s}$ (38). Phamret has been successfully imaged in mammalian cell culture but not to our knowledge in *Drosophila*. Note that the photoconversion only effects a 15-fold change between the two fluorescent states (compare to ~4,000-fold for Dendra2, see below).

2.2.2. Dendra2

Dendra2 is a genetically encoded, monomeric green-to-red fluorophore. It is an improved variant of the original Dendra (39) with increased brightness both before and after photoconversion.

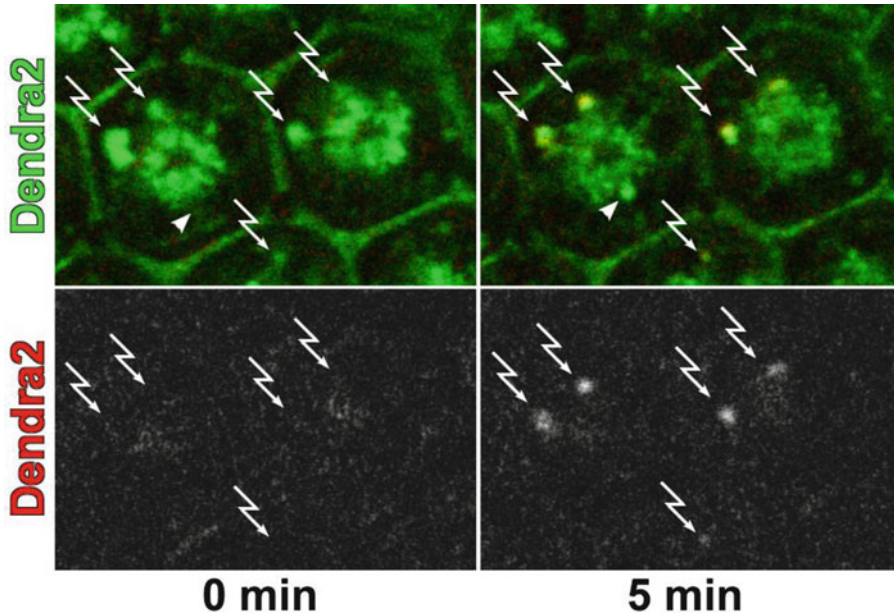


Fig. 3. Live imaging and photoconversion of Dendra2-marked intracellular compartments in the developing *Drosophila* visual system. A Dendra2-n-Syb fusion protein was expressed in the *Drosophila* visual system using GMR-Gal4. Shown is the live preparation of a *Drosophila* eye disc where the *green* and *red* fluorescent spectra are scanned simultaneously. Before photoactivation at 0 min no discernable signal is apparent in the red channel. Over the time course of 5 min, five individual *green* intracellular compartments are photoconverted using UV spot illumination of 10–50 ms (marked by *arrows*). A scan of the same section shows the live scan of these photoconverted compartments in the red channel. The *arrowhead* indicates a new compartment that formed/moved into the focal plane during the 5-min scanning period.

Before photoconversion, Dendra2 is a monomeric fluorescent protein with an excitation maximum at 490 nm and an emission maximum at 507 nm. Dendra2 is designed for photoconversion with both UV as well as normal blue laser (488 nm) illumination (39). After photoconversion, Dendra2 exhibits an excitation maximum of 553 nm and maximal emission at 573 nm. We have generated transgenic flies for the expression of Dendra2, both cytosolic (UAS-Dendra2) as well as tagged intracellular neuronal markers (UAS Dendra2-n-Syb and UAS Dendra2-v100). In our hands, photoconversion with 488 nm laser illumination using spot illumination and 400 Hz conventional or 8,000 Hz resonant laser illumination all lead to Dendra2 bleaching without significant photoconversion. In contrast, photoconversion using 405 nm spot illumination in the millisecond range yields robust Dendra2 photoconversion in *Drosophila* eye-brain preparations (Fig. 3). Notably, Dendra2 and Phamret (above) can be used to simultaneously assay the spatial dynamics of distinct intracellular compartments (40).

2.2.3. PAmCherry

PAmCherry is a recently developed genetically encoded, monomeric red PAFP. It is initially nonfluorescent and can be photoactivated by UV irradiation. PAmCherry is bright enough

for use with PALM and has spectral characteristics that allow two-color PALM by simultaneously imaging with a green PAFP (41). The excitation/emission maxima are at 564/595 nm. So far, expression has only been demonstrated in mammalian cell culture.

2.2.4. *Dronpa Variants*

Dronpa is a genetically encoded, monomeric, PAFP with excitation and emission characteristics similar to those of GFP, but a quantum yield that is 40% higher than that of EGFP (42). Unlike GFP, Dronpa must be activated by irradiation at 405 nm, after which excitation at 488 nm both stimulates fluorescence and deactivates the fluorophore. Further, Dronpa can be reactivated/deactivated multiple times with minimal loss in fluorescence. Dronpa2 and Dronpa3 are half as bright as EGFP; however, they both have greatly enhanced kinetics for both activation and deactivation. This enhancement led to the advent of stroboscopic (S)-PALM, a form of PALM that dramatically shortens data acquisition time (43, 44). bsDronpa has blue-shifted excitation/emission characteristics. This Dronpa variant is activated with 405 nm laser light with excitation/emission maxima at 460 nm and 504 nm, respectively (45). Expression of Dronpa has been demonstrated in mammalian and *Drosophila* S2 cell cultures, but has yet to be demonstrated in vivo in the fly.

2.2.5. *Cyanine Dyes and Rhodamine Amides*

Although genetically encoded PA fluorophores have many advantages, several recently developed photoactivatable fluorescent small molecules have promising potential for use in superresolution fluorescent microscopy, especially in fixed preparations. These include the cyanine dyes (46) and rhodamine amides (47), both of which are photoactivatable and can be fused to a secondary antibody for use in immunohistochemistry. Applications may include antibody internalization, as described in the next section.

2.3. **Extracellular Labeling and Endocytosis**

2.3.1. *Antibody Internalization*

Pulse-chase experiments with specific antibodies are a common method employed to measure receptor endocytosis and intracellular trafficking. The basic idea is to add an antibody against a specific membrane protein or ligand to a live culture. Endocytosis rate and kinetics as well as downstream trafficking (chase) can be measured quantitatively, because the time point and the duration of antibody application (pulse) are defined. The tissue can be fixed after defined time periods to label the internalized antibody with a fluorophore-conjugated secondary antibody as well as other antibodies. For a live imaging variant the primary antibody needs to be conjugated to a fluorophore directly. A detailed protocol has been published for imaging receptor-mediated endocytosis in motor neurons at the *Drosophila* larval NMJ (48). This protocol has been used to study the trafficking of several receptors, including Fasciclin II, Frizzled-2, and Wntless (Wls/Evi) (49–52). Notch receptor endocytosis has been measured in wing discs (53).

2.3.2. Quantum Dots

Quantum dots are nanometer-sized crystals that function as semiconductors. Quantum dots have fluorescent properties that depend on the size and shape of the crystal. Since inorganic semiconductors are toxic and insoluble, the quantum dot core is coated with an amphiphilic material, commonly polyethylene glycol (PEG) (54). Additionally, the polymer coating can be conjugated with tags and proteins of interest. Quantum dots have unique advantages for intracellular labeling; compared to most organic dyes, quantum dots are roughly 20 times as bright, are 100 times as photostable, and have a much narrower emission spectrum, which improves fluorescent isolation in multichannel recordings (55). On the negative side, the bulkiness of quantum dots makes it difficult to label intracellular proteins without interfering with function. Recent technological developments have facilitated access to the cytoplasm (56–58). Despite this limitation, the spectral properties of quantum dots confer the ability to image single molecules on the surface of a cell using conventional fluorescence imaging techniques (59). Additionally, the fate of internalized compartments following a receptor-mediated endocytosis event can be monitored for long periods of time in live culture (60). Indeed, research using quantum dots has led to several recent advances in cell biology (61) and synaptic biology (62).

Quantum dots are currently available in a variety of colors. Commercially available Qdots® are available preconjugated with biological molecules designed for protein labeling. The following list includes some Qdots that can be applied to monitor the fate of cell-surface membrane proteins and endocytosed compartments *in vivo*.

- *Anti-GST*: This Qdot specifically binds the commonly used GST protein tag. In practice, anti-GST Qdots may be helpful for endocytosis experiments using extracellularly GST-tagged protein in live cultures.
- *Secondary antibody*: Qdots are available in a variety of colors and are conjugated with affinity-purified, highly cross-absorbed anti-mouse, rabbit, rat, chicken, or goat antibodies.
- *Amine-derivatized PEG*: This Qdot is sold with a kit that includes the materials and instructions necessary to covalently label this Qdot with primary antibodies. Live imaging of endocytosed Qdots fused to primary antibodies has been demonstrated in rat tumor cells (63).

2.3.3. pHrodo™ Dyes

pHrodo dyes are commercially available derivatives of rhodamine and exhibit increasing fluorescence with decreasing pH. A variety of pHrodo dye conjugates are available; a 10-KDa dextran bead conjugate is useful for the *in vivo* tracking of endocytosed compartments along the endolysosomal pathway. These red fluorescent small molecules are nonfluorescent when added to tissue culture

media at the manufacturer's recommended concentration but become increasingly fluorescent as they are endocytosed and trafficked to lysosomal compartments. Imaging can commence as soon as the dye is added to the tissue culture, since pHrodo dye remaining in the extracellular solution is invisible relative to endocytosed, acidified compartments. This dye could be used in conjunction with the internalization and trafficking assays described above for Qdots.

2.3.4. FM Dyes

FM dyes are lipophilic styryl compounds that are added exogenously to the medium of a live preparation where they quickly incorporate into membranes. Pulse-chase type experiments with FM dyes are widely used to assay membrane trafficking in a variety of tissues. In particular, FM (re-)uptake experiments have been critical in the study of synaptic vesicle cycling (64), including many studies at the *Drosophila* embryonic and larval NMJ (see Chap. 6 for details).

The most commonly used dyes are FM 1-43, FM 2-10, and FM 4-64, which differ mainly in their fluorescence characteristics, but have also been shown to exhibit different kinetics of membrane labeling. FM dyes are highly water soluble, and there they exhibit little fluorescence. FM dye fluorescence strongly increases upon membrane binding. In practice, the dye is dissolved at low concentrations in culture media, the media is added to a tissue culture, and the dye quickly associates with cell membranes where it can now be visualized by fluorescence microscopy. Vesicle cycling is then stimulated by one of the many available methods and the remaining extracellular dye is washed away. Wash efficiency is greatly improved by applying the compound ADVASEP-7, a small molecule added to the culture media that preferentially binds FM dye and quickly removes it from cell membranes. For further information see ref. (64) and Chap. 6.

2.4. Sensors of the Subcellular Environment

Subcellular conditions include pH, levels of nitric oxide (NO), ROS, and calcium concentration, among many others. Some of these features can be measured at the resolution limit of light for individual subcellular compartments in *Drosophila* neural circuit preparations.

2.4.1. Measuring Intracompartamental pH Using LysoTracker® and LysoSensor™

Most intracellular membrane compartments are acidified to varying degrees. For example, synaptic vesicles use the proton motive force resulting from acidification to load neurotransmitter, while acidification of endosomal compartments is directly implicated in signaling through receptor–ligand dissociation and endosomal maturation.

The two probes LysoTracker and LysoSensor use different and complementary strategies to visualize the pH of intracellular compartments. LysoTracker is a fluorescent probe that is added to the culture medium at such low concentrations that background

fluorescence is negligible. We routinely use 100 nM for larval file preparation as well as larval and pupal eye–brain culture. LysoTracker passively diffuses across membranes and selectively accumulates in highly acidified compartments, including lysosomes and autophagosomes, but not early endosomal structures. Hence, LysoTracker labeling of strongly acidified compartments is a function of time. We measure LysoTracker signal 5 min after application. At later time points LysoTracker becomes unreliable, as it may alter the subcellular environment itself. LysoTracker is available with blue, green, yellow, and red spectral properties. In our hands, the fixation of the live LysoTracker signal for subsequent immunolabeling leads to a substantial loss of signal.

In contrast to LysoTracker, LysoSensor is quenched at neutral pH and becomes increasingly fluorescent as pH decreases, becoming maximally fluorescent at pH 5. In other words, while LysoTracker does not change fluorescent properties while accumulating in acidified compartments, LysoSensor does not accumulate, but changes its fluorescent properties as a function of pH. In its practical application, LysoSensor is added to the culture medium similar to LysoTracker but at higher concentrations ($\geq 1 \mu\text{M}$). LysoSensor is available in either blue or green. While use of LysoSensor is a more quantitative way to measure intracompartamental pH, it yields weaker signals in *Drosophila* preparations in our hands.

Notes:

- When using these probes experimentally, results are easier to interpret in genetic mosaics where marked mutant and wild type cells can be used for a quantitative comparison of directly neighboring mutant and control cells. We have made extensive use of LysoTracker in 50/50 MARCM clones (65) in eye–brain cultures (17, 66).
- For whole-brain cultures at any developmental stage, the protective outer membrane must be marginally torn to provide the probes access to cortical cells (66).
- LysoSensor and LysoTracker are also available fused to dextran beads for experiments where an initial endocytosis event is desirable.
- Images should be recorded within the first 5 min after adding these probes to the culture due to a potentially confounding alkalizing effect.

2.4.2. Measuring
Intracompartamental
pH Using Synapto-pHluorin

pHluorin is a genetically encoded, pH-sensitive GFP variant that exhibits increasing fluorescence intensity with increasing luminal pH, fluorescing minimally at pH 5 and maximally at pH 8 (67). In functional studies of *Drosophila* neurons, pHluorin fused to the luminal end of synaptobrevin (synapto-pHluorin) has been used

to image synaptic vesicle fusion, an event that results in the neutralization of an otherwise acidified synaptic vesicle and a consequential increase in synapto-pHluorin fluorescence (34). We have recently used synapto-pHluorin in *Drosophila* neurons to measure the luminal pH of early endosomes in live eye-brain culture by acquiring confocal images before and after neutralization of the lumen (17). By targeting pHluorin-tagged molecules to specific intracellular compartments, luminal pH can be measured in a targeted manner.

2.4.3. HyPer: Measuring Reactive Oxygen Species In Vivo

This ratiometric, genetically encoded hydrogen peroxide sensor has spectral characteristics similar to YFP and can be tagged to a gene of interest for targeted subcellular localization (68). HyPer effectively senses ROS in vivo without emitting ROS on its own. Expression of this FP has been demonstrated in mammalian cell culture (69) and Zebrafish (70), but not to our knowledge in *Drosophila*.

2.4.4. GCaMP3: The Latest in Calcium-Sensing

Calcium ion concentrations modulate a plethora of cell biological events; for a review of calcium signaling in cell biology, see ref. (71). Calcium influx upon synaptic activation has traditionally been the most powerful approach used to directly visualize and image synaptic activity. GCaMP3 is a green fluorescent, genetically encoded calcium sensor that exhibits increasing fluorescent intensity in direct proportion with increasing calcium ion concentrations. GCaMP3 has been used to report neural activity in model organisms including *Drosophila* (72). However, its application could theoretically extend into the realm of other Ca-dependent cell biological processes by targeting GCaMP3 to a specific subcellular region of interest.

2.4.5. CuFL: A Copper-Based Fluorescent Probe for Nitric Oxide

Nitric oxide (NO) has been implicated in the signaling program of *Drosophila* optic lobe development (23). CuFL, the first direct sensor for NO levels in living cells, was recently introduced and might prove useful in further cell biological studies involving NO (73). This fluorescein-based small molecule diffuses freely across membranes and fluoresces in the green spectrum only in the presence of NO.

3. Examples for Imaging of Intracellular Trafficking in Neural Circuits

Intracellular trafficking underlies many aspects of the development and function of neural circuits. In order to establish meaningful synaptic connections, neurons must present or interpret guidance cues at the right place and time. After connections are made,

activity-dependent and -independent modifications require the regulated delivery or removal of channels, receptors, and many other signaling proteins. Finally, neuronal degeneration typically commences with diminished synaptic function and the accumulation of undegraded proteins. In short, intracellular trafficking affects all stages in the life of a neural circuit from development to maintenance to degeneration. In this section, we highlight a few examples that illuminate the importance and application of subcellular resolution imaging for the formation, function, and maintenance of neural circuits.

3.1. Intracellular Trafficking in Circuit Formation

Once regarded as merely passive transport machinery, intracellular vesicle trafficking is now known to play instructive roles in most aspects of developmental biology, including signal transduction, asymmetric cell division, cell fate specification and cell growth. Prominent examples include the regulation of cellular differentiation by endo-/exocytosis of the Notch ligand Delta (reviewed in refs. (74–76)) and the regulation of synaptic plasticity by AMPA receptor trafficking (reviewed in refs. (77, 78)). Comparatively little is known about the function of intracellular trafficking compartments during axon pathfinding, target selection, and synapse formation (79). This is surprising because a general feature of guidance receptors known to mediate synaptic targeting choices is precise spatiotemporal regulation, i.e., they must be presented at the right time and place on the membrane to convey meaningful synapse formation signals during brain wiring. This problem is amplified by the number of guidance receptors or their isoforms that need to be spatiotemporally regulated during brain development.

Perhaps the best characterized example of an instructive role of guidance receptor trafficking during axon targeting is the regulation of the guidance receptor Robo by the endosomal sorting receptor commissureless (80–82). Commissureless (Comm) is required cell-autonomously in ipsilateral pioneer neurons in the *Drosophila* embryo in order to allow midline crossing of these neurons. Robo is the receptor for the repellent Slit. In order to allow midline crossing, Comm temporarily diverts the Robo receptor from the Golgi to the endosomal/lysosomal pathway. Comm thus ensures a precise spatiotemporal developmental program to establish correct neuronal connectivity (82). Live imaging of the trafficking of a Robo-green fluorescent protein (GFP) fusion in living embryos demonstrated that Comm prevents the delivery of Robo-GFP to the growth cone (81).

Similarly, a study on intraaxonal patterning demonstrated a requirement for endocytosis in the spatiotemporal localization of the guidance receptors Robo3 and Derailed (31). Using a live imaging approach with fluorescently labeled receptors that include Fluorescence Recovery After Photobleaching (FRAP), the same study also showed that transmembrane proteins are

mobile within their compartment but less mobile at intraaxonal compartment boundaries.

In more general terms, endosomal compartments can function as signaling hubs that control the activation and downregulation of guidance receptors (83, 84). We have recently shown that experimental control and simultaneous imaging of endolysosomal trafficking in eye–brain complexes *in vivo* provides a means to visualize what guidance receptors are actively “cycled” at a given time in a specific neuronal subcellular domain, e.g., the synapse or cell body (64).

3.2. Intracellular Trafficking in Circuit Function

Since synaptic function is reviewed elsewhere in this book (Chap. 6), we only briefly discuss the key intracellular trafficking events of relevance for subcellular resolution imaging. The key features of synaptic function with respect to imaging are: First, the conduction of an electrical potential, which can be imaged using voltage-dependent dyes and probes not discussed in this chapter. Second, calcium-influx at the synapse provides a fast and reliable readout for both the Ca-sensing machinery that triggers neurotransmitter release as well as the experimentalist imaging synaptic activity (see discussion of GCaMP3 (85) in Sect. 2). Third, neurotransmitter release at chemical synapses is regulated by the synaptic vesicle cycle, a large-scale intracellular trafficking machinery that closely intersects with the secretory pathway and endosomal trafficking. Synaptic vesicle exocytosis and endocytosis can be imaged with a variety of powerful genetically encoded or exogenously applied probes. One of the most successfully applied tools for the study of *Drosophila* circuitry function is the genetically encoded exocytic probe synapto-pHluorin (66, 86). Since synapto-pHluorin can be expressed anywhere in the fly nervous system using the Gal4/UAS system, its applicability is limited mostly by the amount and detectability of synchronous fluorescence increase at active synapses in a given circuit. Of more limited use for circuit function are exogenously applied probes including FM dyes. However, any preparation that allows such probes to freely diffuse into the synaptic cleft can turn these probes into powerful assays for synaptic function and underlying intracellular trafficking.

3.3. Intracellular Trafficking in Circuit Degeneration

Numerous subcellular mechanisms that lead to neurodegeneration have been proposed, including axonal transport, protein aggregation, mitochondrial dysfunction, excitotoxicity, and intracellular transport (87–89). Many of these mechanisms have benefited greatly in recent years from the ability to visualize their dynamics at subcellular resolution in neuronal circuit preparations *in vivo*.

Axonal transport is critical for the cell body to communicate with the cell periphery. The highly polarized morphology and the differential requirement of membrane components in neurons represent a challenge for the trafficking machinery to correctly deliver cargos. Defects in axon transport have been implicated in the

neurodegeneration in Alzheimer Disease, amyotrophic lateral sclerosis, and the polyglutamine diseases (90–93). In *Drosophila*, disruption of microtubule motor proteins kinesin1 or dynactin leads to accumulated cargos including vesicles, synaptic membrane proteins, and mitochondria. The axonal swellings (“organelle jams”) are thought to block axon transport, resulting in neuromuscular defects and disruption of neuronal organization.

The removal of subcellular “debris” is essential for maintaining functional neurons. Neurons use several approaches for dispose of toxic protein aggregates and damaged organelles. These clearance mechanisms include targeting proteins for proteasomal degradation and transporting substrates such as protein complexes and organelles to lysosomes and autophagosomes for subsequent degradation (94). In recent years *Drosophila* has been employed as a model system to study the basic cell biological machinery underlying the subcellular defects observed in many neurodegenerative diseases. For example, defective lysosomal function in the mutant for the lysosomal sugar carrier *spinster/benchwarmer* (95) or the protective chaperone NMNAT (96) cause neurodegeneration and provide genetic inroads into lysosomal degradation and misfolded protein responses, respectively. We have recently reported a neuron-specific intracellular degradation pathway based on the function of the neuronal v-ATPase subunit V0a1 (17). Loss of v0a1 leads to adult-onset degeneration in photoreceptors and sensitizes neurons to neurotoxic insults, including human tau and Aβ proteins (97). The identification and characterization of this neuronal degradation mechanism was performed in eye–brain live culture and fixed preparations, using many of the techniques described above, including resonant confocal live imaging of Lysotracker, synaptophluorin, and other probes.

Autophagy plays a potentially protective role in neurodegeneration. In mammals, knockouts of autophagy-related genes result in intra-neuronal aggregates and neurodegeneration (98, 99). In *Drosophila*, *atg7* mutants display protein aggregation and neuronal degeneration in aged brains, indicating that autophagy plays a neuroprotective role in the CNS (100, 101). Numerous fluorescently tagged autophagy reporters exist, including Atg8-GFP (102).

Acknowledgments

We thank all members of the Hiesinger lab for discussion. We apologize to all of our colleagues whose work was not discussed because of space constraints or our shortcomings. Our work is supported by grants from the Welch Foundation (I-1657), a grant from the

Cancer Prevention Research Institute of Texas (CPRIT) and the National Institute of Health (NEI/NIH RO1018884). PRH is a Eugene McDermott Scholar in Biomedical Research at UT Southwestern Medical Center.

References

- Schermelleh L, Heintzmann R, Leonhardt H (2010) A guide to super-resolution fluorescence microscopy. *J Cell Biol* 190:165
- Pawley J (2006) Handbook of biological confocal microscopy, 3rd edn. Springer, Berlin
- Hell SW (2007) Far-field optical nanoscopy. *Science* 316:1153–1158
- Gibson SF, Lanni F (1992) Experimental test of an analytical model of aberration in an oil-immersion objective lens used in three-dimensional light microscopy. *J Opt Soc Am A* 9:154–166
- Richardson WH (1972) Bayesian-based iterative method of image restoration. *J Opt Soc Am* 62:55–59
- Holmes TJ (1988) Maximum-likelihood image restoration adapted for non-coherent optical imaging. *J Opt Soc Am A* 5:666–673
- Hiesinger PR, Scholz M, Meinertzhagen IA, Fischbach KF, Obermayer K (2001) Visualization of synaptic markers in the optic neuropils of *Drosophila* using a new constrained deconvolution method. *J Comp Neurol* 429:277–288
- Borlinghaus RT (2006) MRT letter: high speed scanning has the potential to increase fluorescence yield and to reduce photobleaching. *Microsc Res Tech* 69:689–692
- Graf R, Rietdorf J, Zimmermann T (2005) Live cell spinning disk microscopy. *Adv Biochem Eng Biotechnol* 95:57–75
- Nakano A (2002) Spinning-disk confocal microscopy—a cutting-edge tool for imaging of membrane traffic. *Cell Struct Funct* 27:349–355
- Helmchen F, Denk W (2002) New developments in multiphoton microscopy. *Curr Opin Neurobiol* 12:593–601
- Huang B, Babcock H, Zhuang X (2010) Breaking the diffraction barrier: super-resolution imaging of cells. *Cell* 143:1047–1058
- Betzig E, Patterson GH, Sougrat R, Lindwasser OW, Olenych S, Bonifacino JS, Davidson MW, Lippincott-Schwartz J, Hess HF (2006) Imaging intracellular fluorescent proteins at nanometer resolution. *Science* 313:1642–1645
- Zhuang X (2009) Nano-imaging with storm. *Nat Photonics* 3:365–367
- Aldaz S, Escudero LM, Freeman M (2010) Live imaging of *Drosophila* imaginal disc development. *Proc Natl Acad Sci U S A* 107:14217–14222
- Brink D, Gilbert M, Auld V (2009) Visualizing the live *Drosophila* glial-neuromuscular junction with fluorescent dyes. *J Vis Exp* 27:1154
- Williamson W, Wang D, Haberman A, Hiesinger P (2010) A dual function of V0-ATPase a1 provides an endolysosomal degradation mechanism in *Drosophila melanogaster* photoreceptors. *J Cell Biol* 189:885
- Williamson WR, Hiesinger PR (2010) Preparation of developing and adult *Drosophila* brains and retinae for live imaging. *J Vis Exp* 37:1936
- Semmelhack JL, Wang JW (2009) Select *Drosophila* glomeruli mediate innate olfactory attraction and aversion. *Nature* 459:218–223
- Wang JW, Wong AM, Flores J, Vosshall LB, Axel R (2003) Two-photon calcium imaging reveals an odor-evoked map of activity in the fly brain. *Cell* 112:271–282
- Featherstone DE, Chen K, Broadie K (2009) Harvesting and preparing *Drosophila* embryos for electrophysiological recording and other procedures. *J Vis Exp* 27:1347
- Kittel RJ, Wichmann C, Rasse TM, Fouquet W, Schmidt M, Schmid A, Wagh DA, Pawlu C, Kellner RR, Willig KI, Hell SW, Buchner E, Heckmann M, Sigrist SJ (2006) Bruchpilot promotes active zone assembly, Ca²⁺ channel clustering, and vesicle release. *Science* 312:1051–1054
- Gibbs S, Truman J (1998) Nitric oxide and cyclic GMP regulate retinal patterning in the optic lobe of *Drosophila*. *Neuron* 20:83–93
- Ayaz D, Leyssen M, Koch M, Yan J, Srahna M, Sheeba V, Fogle KJ, Holmes TC, Hassan BA (2008) Axonal injury and regeneration in the adult brain of *Drosophila*. *J Neurosci* 28:6010–6021
- Suh GS, Wong AM, Hergarden AC, Wang JW, Simon AF, Benzer S, Axel R, Anderson DJ (2004) A single population of olfactory sensory neurons mediates an innate avoidance behaviour in *Drosophila*. *Nature* 431:854–859
- Stowers RS, Schwarz TL (1999) A genetic method for generating *Drosophila* eyes

- composed exclusively of mitotic clones of a single genotype. *Genetics* 152:1631–1639
27. Newsome TP, Asling B, Dickson BJ (2000) Analysis of *Drosophila* photoreceptor axon guidance in eye-specific mosaics. *Development* 127:851–860
 28. Chotard C, Leung W, Salecker I (2005) glial cells missing and *gcm2* cell autonomously regulate both glial and neuronal development in the visual system of *Drosophila*. *Neuron* 48:237–251
 29. Shcherbo D, Murphy C, Ermakova G, Solovieva E, Chepurnykh T, Shcheglov A, Verkhusha V, Pletnev V, Hazelwood K, Roche P (2009) Far-red fluorescent tags for protein imaging in living tissues. *Biochem J* 418:567
 30. Ai H, Shaner N, Cheng Z, Tsien R, Campbell R (2007) Exploration of new chromophore structures leads to the identification of improved blue fluorescent proteins. *Biochemistry* 46:5904–5910
 31. Katsuki T, Ailani D, Hiramoto M, Hiromi Y (2009) Intra-axonal patterning: intrinsic compartmentalization of the axonal membrane in *Drosophila* neurons. *Neuron* 64:188–199
 32. Marks K, Nolan G (2006) Chemical labeling strategies for cell biology. *Nat Methods* 3: 591–596
 33. Marek K, Davis G (2002) Transgenically encoded protein photoinactivation (FLAsH-FALI): acute inactivation of synaptotagmin I. *Neuron* 36:805–813
 34. Poskanzer K, Marek K, Sweeney S, Davis G (2003) Synaptotagmin I is necessary for compensatory synaptic vesicle endocytosis in vivo. *Nature* 426:559–563
 35. Venken K, Kasprowitz J, Kuenen S, Yan J, Hassan B, Verstreken P (2008) Recombinase-mediated tagging of *Drosophila* genomic constructs for in vivo localization and acute protein inactivation. *Nucleic Acids Res* 36:e114
 36. Bulina ME, Chudakov DM, Britanova OV, Yanushevich YG, Staroverov DB, Chepurnykh TV, Merzlyak EM, Shkrob MA, Lukyanov S, Lukyanov KA (2006) A genetically encoded photosensitizer. *Nat Biotechnol* 24:95–99
 37. Del Bene F, Wyart C, Robles E, Tran A, Looger L, Scott EK, Isacoff EY, Baier H (2010) Filtering of visual information in the tectum by an identified neural circuit. *Science* 330:669–673
 38. Matsuda T, Miyawaki A, Nagai T (2008) Direct measurement of protein dynamics inside cells using a rationally designed photoconvertible protein. *Nat Methods* 5:339–345
 39. Gurskaya N, Verkhusha V, Shcheglov A, Staroverov D, Chepurnykh T, Fradkov A, Lukyanov S, Lukyanov K (2006) Engineering of a monomeric green-to-red photoactivatable fluorescent protein induced by blue light. *Nat Biotechnol* 24:461–465
 40. Chudakov D, Lukyanov S, Lukyanov K (2007) Tracking intracellular protein movements using photoswitchable fluorescent proteins PS-CFP2 and Dendra2. *Nat Protoc* 2:2024–2032
 41. Subach F, Patterson G, Manley S, Gillette J, Lippincott-Schwartz J, Verkhusha V (2009) Photoactivatable mCherry for high-resolution two-color fluorescence microscopy. *Nat Methods* 6:153–159
 42. Ando R, Mizuno H, Miyawaki A (2004) Regulated fast nucleocytoplasmic shuttling observed by reversible protein highlighting. *Science* 306:1370
 43. Ando R, Flors C, Mizuno H, Hofkens J, Miyawaki A (2007) Highlighted generation of fluorescence signals using simultaneous two-color irradiation on Dronpa mutants. *Biophys J* 92:L97–L99
 44. Flors C, Hotta J, Uji-i H, Dedecker P, Ando R, Mizuno H, Miyawaki A, Hofkens J (2007) A stroboscopic approach for fast photoactivation-localization microscopy with Dronpa mutants. *J Am Chem Soc* 129:13970–13977
 45. Andresen M, Stiel A, Fölling J, Wenzel D, Schönle A, Egner A, Eggeling C, Hell S, Jakobs S (2008) Photoswitchable fluorescent proteins enable monochromatic multilabel imaging and dual color fluorescence nanoscopy. *Nat Biotechnol* 26:1035–1040
 46. Bates M, Huang B, Dempsey G, Zhuang X (2007) Multicolor super-resolution imaging with photo-switchable fluorescent probes. *Science* 317:1749
 47. Bossi M, Fölling J, Belov V, Boyarskiy V, Medda R, Egner A, Eggeling C, Schonle A, Hell S (2008) Multicolor far-field fluorescence nanoscopy through isolated detection of distinct molecular species. *Nano Lett* 8: 2463–2468
 48. Ramachandran P, Budnik V (2010) Internalization and trafficking assay for *Drosophila* larvae. *Cold Spring Harb Protoc* 2010(8):pdb.prot5472
 49. Ataman B, Ashley J, Gorczyca D, Gorczyca M, Mathew D, Wichmann C, Sigrist S, Budnik V (2006) Nuclear trafficking of *Drosophila* Frizzled-2 during synapse development requires the PDZ protein dGRIP. *Proc Natl Acad Sci U S A* 103(20):7841–7846
 50. Korkut C, Ataman B, Ramachandran P, Ashley J, Barria R, Gherbesi N, Budnik V (2009) Trans-synaptic transmission of vesicular Wnt

- signals through Evi/Wntless. *Cell* 139:393–404
51. Mathew D, Popescu A, Budnik V (2003) *Drosophila* amphiphysin functions during synaptic Fasciclin II membrane cycling. *J Neurosci* 23:10710
 52. Mathew D, Ataman B, Chen J, Zhang Y, Cumberledge S, Budnik V (2005) Wingless signaling at synapses is through cleavage and nuclear import of receptor DFrizzled2. *Science* 310:1344
 53. Maitra S, Kulikauskas RM, Gavilan H, Fehon RG (2006) The tumor suppressors Merlin and Expanded function cooperatively to modulate receptor endocytosis and signaling. *Curr Biol* 16(7):702–709
 54. Walling M, Novak J, Shepard J (2009) Quantum dots for live cell and in vivo imaging. *Int J Mol Sci* 10:441
 55. Chan W, Nie S (1998) Quantum dot bioconjugates for ultrasensitive nonisotopic detection. *Science* 281:2016
 56. Jablonski A, Humphries W IV, Payne C (2008) Pyrenebutyrate-mediated delivery of quantum dots across the plasma membrane of living cells. *J Phys Chem B* 113:405–408
 57. Kim B, Jiang W, Oreopoulos J, Yip C, Rutka J, Chan W (2008) Biodegradable quantum dot nanocomposites enable live cell labeling and imaging of cytoplasmic targets. *Nano Lett* 8:3887–3892
 58. Delehanty J, Mattoussi H, Medintz I (2009) Delivering quantum dots into cells: strategies, progress and remaining issues. *Anal Bioanal Chem* 393:1091–1105
 59. Jaqaman K, Loerke D, Mettlen M, Kuwata H, Grinstein S, Schmid S, Danuser G (2008) Robust single-particle tracking in live-cell time-lapse sequences. *Nat Methods* 5:695–702
 60. Cui B, Wu C, Chen L, Ramirez A, Bearer E, Li W, Mobley W, Chu S (2007) One at a time, live tracking of NGF axonal transport using quantum dots. *Proc Natl Acad Sci U S A* 104:13666
 61. Pinaud F, Clarke S, Sittner A, Dahan M (2010) Probing cellular events, one quantum dot at a time. *Nat Methods* 7:275–285
 62. Triller A, Choquet D (2008) New concepts in synaptic biology derived from single-molecule imaging. *Neuron* 59:359–374
 63. Tada H, Higuchi H, Wanatabe T, Ohuchi N (2007) In vivo real-time tracking of single quantum dots conjugated with monoclonal anti-HER2 antibody in tumors of mice. *Cancer Res* 67:1138
 64. Gaffield M, Betz W (2007) Imaging synaptic vesicle exocytosis and endocytosis with FM dyes. *Nat Protoc* 1:2916–2921
 65. Lee T, Luo L (1999) Mosaic analysis with a repressible cell marker for studies of gene function in neuronal morphogenesis. *Neuron* 22:451–461
 66. Williamson WR, Yang T, Terman JR, Hiesinger PR (2010) Guidance receptor degradation is required for neuronal connectivity in the *Drosophila* nervous system. *PLoS Biol* 8:e1000553
 67. Miesenböck G, De Angelis D, Rothman J (1998) Visualizing secretion and synaptic transmission with pH-sensitive green fluorescent proteins. *Nature* 394:192–195
 68. Belousov V, Fradkov A, Lukyanov K, Staroverov D, Shakhbazov K, Terskikh A, Lukyanov S (2006) Genetically encoded fluorescent indicator for intracellular hydrogen peroxide. *Nat Methods* 3:281–286
 69. Wu R, Ma Z, Liu Z, Terada L (2010) Nox4-derived H₂O₂ mediates endoplasmic reticulum signaling through local Ras activation. *Mol Cell Biol* 30:3553
 70. Niethammer P, Grabher C, Look A, Mitchison T (2009) A tissue-scale gradient of hydrogen peroxide mediates rapid wound detection in zebrafish. *Nature* 459:996–999
 71. Clapham D (2007) Calcium signaling. *Cell* 131:1047–1058
 72. Seelig J, Chiappe M, Lott G, Dutta A, Osborne J, Reiser M, Jayaraman V (2010) Two-photon calcium imaging from head-fixed *Drosophila* during optomotor walking behavior. *Nat Methods* 7(7):535–540
 73. Lim M, Xu D, Lippard S (2006) Visualization of nitric oxide in living cells by a copper-based fluorescent probe. *Nat Chem Biol* 2:375–380
 74. Fischer JA, Eun SH, Doolan BT (2006) Endocytosis, endosome trafficking, and the regulation of *Drosophila* development. *Annu Rev Cell Dev Biol* 22:181–206
 75. Chitnis A (2006) Why is delta endocytosis required for effective activation of notch? *Dev Dyn* 235:886–894
 76. Le Borgne R, Bardin A, Schweisguth F (2005) The roles of receptor and ligand endocytosis in regulating Notch signaling. *Development* 132:1751–1762
 77. Greger IH, Esteban JA (2007) AMPA receptor biogenesis and trafficking. *Curr Opin Neurobiol* 17(3):287–297
 78. Nicoll RA, Tomita S, Bredt DS (2006) Auxiliary subunits assist AMPA-type glutamate receptors. *Science* 311:1253–1256

79. Chan CC, Epstein D, Hiesinger PR (2011) Intracellular trafficking in *Drosophila* visual system development: a basis for pattern formation through simple mechanisms. *Dev Neurosci* 71(12):1227–1245
80. Keleman K, Rajagopalan S, Cleppien D, Teis D, Paiha K, Huber LA, Technau GM, Dickson BJ (2002) Comm sorts robo to control axon guidance at the *Drosophila* midline. *Cell* 110:415–427
81. Keleman K, Ribeiro C, Dickson BJ (2005) Comm function in commissural axon guidance: cell-autonomous sorting of Robo in vivo. *Nat Neurosci* 8:156–163
82. Dickson BJ, Gilestro GF (2006) Regulation of commissural axon pathfinding by slit and its Robo receptors. *Annu Rev Cell Dev Biol* 22:651–675
83. O'Donnell M, Chance RK, Bashaw GJ (2009) Axon growth and guidance: receptor regulation and signal transduction. *Annu Rev Neurosci* 32:383–412
84. Seto ES, Bellen HJ, Lloyd TE (2002) When cell biology meets development: endocytic regulation of signaling pathways. *Genes Dev* 16:1314–1336
85. Tian L, Hires SA, Mao T, Huber D, Chiappe ME, Chalasani SH, Petreanu L, Akerboom J, McKinney SA, Schreiter ER, Bargmann CI, Jayaraman V, Svoboda K, Looger LL (2009) Imaging neural activity in worms, flies and mice with improved GCaMP calcium indicators. *Nat Methods* 6:875–881
86. Ng M, Roorda RD, Lima SQ, Zemelman BV, Morcillo P, Miesenbock G (2002) Transmission of olfactory information between three populations of neurons in the antennal lobe of the fly. *Neuron* 36:463–474
87. Lu B, Vogel H (2009) *Drosophila* models of neurodegenerative diseases. *Ann Rev Pathol* 4:315–342
88. Lessing D, Bonini N (2009) Maintaining the brain: insight into human neurodegeneration from *Drosophila melanogaster* mutants. *Nat Rev Genet* 10:359–370
89. De Vos K, Grierson A, Ackerley S, Miller C (2008) Role of axonal transport in neurodegenerative diseases. *Neuroscience* 31:151
90. Williamson TL, Cleveland DW (1999) Slowing of axonal transport is a very early event in the toxicity of ALS-linked SOD1 mutants to motor neurons. *Nat Neurosci* 2:50–56
91. LaMonte BH, Wallace KE, Holloway BA, Shelly SS, Ascano J, Tokito M, Van Winkle T, Howland DS, Holzbaur EL (2002) Disruption of dynein/dynactin inhibits axonal transport in motor neurons causing late-onset progressive degeneration. *Neuron* 34:715–727
92. Puls I, Jonnakuty C, LaMonte BH, Holzbaur EL, Tokito M, Mann E, Floeter MK, Bidus K, Drayna D, Oh SJ, Brown RH Jr, Ludlow CL, Fischbeck KH (2003) Mutant dynactin in motor neuron disease. *Nat Genet* 33:455–456
93. Gunawardena S, Goldstein LS (2005) Polyglutamine diseases and transport problems: deadly traffic jams on neuronal highways. *Arch Neurol* 62:46–51
94. Garcia-Arencibia M, Hochfeld WE, Toh PP, Rubinsztein DC (2010) Autophagy, a guardian against neurodegeneration. *Semin Cell Dev Biol* 21:691–698
95. Dermaut B, Norga KK, Kania A, Verstreken P, Pan H, Zhou Y, Callaerts P, Bellen HJ (2005) Aberrant lysosomal carbohydrate storage accompanies endocytic defects and neurodegeneration in *Drosophila* benchwarmer. *J Cell Biol* 170:127–139
96. Zhai RG, Cao Y, Hiesinger PR, Zhou Y, Mehta SQ, Schulze KL, Verstreken P, Bellen HJ (2006) *Drosophila* NMNAT maintains neural integrity independent of its NAD synthesis activity. *PLoS Biol* 4:e416
97. Williamson WR, Hiesinger PR (2010) On the role of v-ATPase V0a1-dependent degradation in Alzheimer disease. *Commun Integr Biol* 3:604–607
98. Komatsu M, Waguri S, Chiba T, Murata S, Iwata J, Tanida I, Ueno T, Koike M, Uchiyama Y, Kominami E, Tanaka K (2006) Loss of autophagy in the central nervous system causes neurodegeneration in mice. *Nature* 441:880–884
99. Hara T, Nakamura K, Matsui M, Yamamoto A, Nakahara Y, Suzuki-Migishima R, Yokoyama M, Mishima K, Saito I, Okano H, Mizushima N (2006) Suppression of basal autophagy in neural cells causes neurodegenerative disease in mice. *Nature* 441:885–889
100. Juhasz G, Erdi B, Sass M, Neufeld TP (2007) Atg7-dependent autophagy promotes neuronal health, stress tolerance, and longevity but is dispensable for metamorphosis in *Drosophila*. *Genes Dev* 21:3061–3066
101. McPhee CK, Baehrecke EH (2009) Autophagy in *Drosophila melanogaster*. *Biochim Biophys Acta* 1793:1452–1460
102. Chang YY, Neufeld TP (2009) An Atg1/Atg13 complex with multiple roles in TOR-mediated autophagy regulation. *Mol Biol Cell* 20:2004–2014